



Influential analysis of geometrical parameters on falling-film thickness and distribution of sheet flow outside horizontal tube

Qinggong Qiu, Xiaocui Zhang, Xiaojing Zhu, Shenglin Quan*, Shengqiang Shen

School of Energy and Power Engineering, Dalian University of Technology, 116024 Dalian, China, Tel. +86 13998572573, Fax +86 411 84708460, email: qqgong@dlut.edu.cn (Q. Qiu), zhangxiaocui@dlut.edu.cn (X. Zhang), zhuxiaojing@dlut.edu.cn (X. Zhu), slquan@dlut.edu.cn (S. Quan), aabshen@dlut.edu.cn (S. Shen)

Received 24 November 2017; Accepted 1 July 2018

ABSTRACT

The flow characteristics of falling film outside horizontal round- and elliptical tubes are simulated based on a finite volume solution to the Navier–Stokes equations coupled with the volume of fluid method at a liquid–vapor interface. A two-dimensional multi-phase flow model is developed using adiabatic conditions for the sheet flow, where the tube walls are assumed, in practice, to be completely wetted by liquid water. The effects of the tube arrangement, inter-tube spacing, liquid feeder height, and tube shape on the thickness distribution of a liquid film in the circumferential direction are presented in detail. The results show that the tube arrangement has little effect on the first row of tubes, and a significant effect on the second row of tubes, under a fixed fluid flow density. The film thickness decreases with an increase in the inter-tube spacing. The higher feeder height leads to a thinner film. In addition, the film thickness outside the elliptical tube is more unique compared with that of a circular tube. The lesser effect of wake turbulence and the larger developed film region outside an elliptical tube have more advantages in terms of the heat transfer process. The results can provide the basis and guidance for further research on and development of an efficient horizontal-tube falling-film evaporator.

Keywords: Sheet flow; Two-phase flow; Geometrical structure parameters; Film thickness

1. Introduction

A horizontal-tube falling-film evaporator (HSFFE) is an efficient energy conservation device, and has been widely used in practical production processes. Compared with conventional evaporators, the falling-film evaporation technique has more significant advantages, including a higher heat-transfer coefficient, a smaller temperature difference, and an easier arrangement during a multi-effect distillation process. The falling liquid film evenly distributes outside the horizontal tube, and can deal well with non-condensable gases.

In an HSFFE, the liquid falls through the horizontal tube bundle. The hot liquid inside the tubes is cooled by falling liquid outside the tubes, and heat transfer occurs from the falling film covering the tubes. In addition, a mass transfer

occurs during the period of droplet formation. The characteristics of the falling film influence the efficiency of the heat and mass transfer. A study of the falling-film flow characteristics and film distribution covering the tubes is significant. The liquid film is estimated to be uniform and thin with a certain feeding supply. However, a dry out or an extensive amount of film will occur without a proper feeding supply. Furthermore, the waves or ripples of the liquid film appearing during the falling-film evolution process will clearly affect the heat transfer efficiency.

The falling-film evolution includes the droplet formation, detachment, and impact, among other factors. Some corresponding parameters have an effect on the film flow characteristics, such as the geometrical features, liquid flow rate, non-condensable gases, and operating conditions. A lot of scientists and researchers are interested in these, and their researches have determined the flow and thermal regimes. Nusselt [1] analyzed the evaporation process

*Corresponding author.

when a cooling liquid flows along the surface of a horizontal tube. Based on Nusselt's research, Rogers and Goindi [2] studied the film thickness experimentally and obtained a calculation formula for use in heat transfer cases. Hu and Jacobi [3] also investigated the flow patterns of falling film. In their research, some parameters were analyzed to show the flow characteristics and pattern transitions. They also presented new equations to distinguish the flow patterns based on a large amount of experimental data. Slesarenko [4] conducted a number of experiments on the falling-film evaporation process. The author chose different types of tubes for a study on the film distribution and heat transfer coefficient. The heat flux, flow rate, and tube size were considered comprehensively in these experiments. Ribatski [5] provided an experimental review of the two-phase flow characteristics and heat transfer methods. Xu [6,7] studied the liquid flow characteristics and film distribution outside horizontal tubes. The heat transfer coefficients in a falling-film evaporator were obtained through their experiments. Harikrishnan [8,9] studied the heat and mass transfer models of falling film tubes both analytically and experimentally. The author concluded that the peak value of the mass flux decreases with an increase in the flow rate, and then increases when the film reaches a depth of 40% of the film thickness. Moreover, the overall heat and mass transfer coefficients increase with the mass flow rate. Hou [10] comprehensively studied the distribution characteristics of the falling film thickness. Here, the Reynolds number varied from 150 to 800, and the inter-tube spacing ranged from 10 to 40 mm. The author also compared these experiment results with Nusselt's theory and proposed a new correlation to predict the film thickness. Mu [11] built a three-dimensional model to investigate the characteristics of a fluid flow and film spread. Experiments were also carried out to explore the influencing factors of the falling film flow and spread in detail. The author also studied the heat transfer coefficient of falling-film evaporation with different working fluids. Chen [12] presented the film thickness of seawater using laser-induced fluorescence technology, and analyzed the collision of two adjacent columns, which caused a liquid bump in the middle of two columns. In our previous work [13], the film characteristics outside a round horizontal tube were numerically investigated. In this previous work, the Reynolds number varied from 100 to 1000, and the inter-tube spacing increased from 6 to 19 mm. The effects of the diameter size on the film thickness at different flow rates were also discussed. Subramaniam [14] numerically studied the heat and mass transfer in horizontal bundles, and simulated the process of falling liquid at a 3D dimensional resolution using the volume of fluid (VOF) technique. Aguilar [15] presented an experiment study on falling film absorption. In the author's study, the Reynolds number varied from 108 to 246, and the flow patterns were observed during the experiments. Bustamante [16] studied the flow mechanisms using a bundle of three tubes. The droplet and wave characteristics were measured using a semi-autonomous image analysis method. Qi [17] numerically and experimentally studied the effect of the spray density and the ellipticity on the thickness of a single tube of liquid film. Saleh and Ormiston [18] used a segregated solution method based on a finite volume approach and the full 2D elliptic Navier-Stokes equations to study the character-

istics of liquid film thickness, heat transfer, and temperature difference. Zhao [19] numerically studied the effects of film flow rate, heat flux, inlet liquid temperature, tube diameter and liquid distributor height on sub-cooled falling film heat transfer outside a horizontal circular tube.

Based on the above researches, the distribution characteristics based on the thickness of the falling film, along with the heat and mass transfer characteristics of horizontal tube bundles, were continuously and systematically studied. However, most of the above researches focused on a round tube rather than an elliptical tube. Fewer researchers focused on the effects of the geometrical characteristics on the thermal transfer process. This paper presents the unique advantages of a falling-film heat transfer when compared with that of a round tube, which can be used in the design of a multi-effect distillation system. The commercial CFD code, Fluent 6.3.26, was used to simulate the distribution characteristics based on the thickness of the falling film over horizontal tubes. The objectives of this study are to analyze the effects of the geometrical arrangement, including the tube arrangement, inter-tube spacing, liquid feeder height, and tube shape, and to determine the corresponding mechanism involved in the flowing process of a falling film.

2. Numerical model

2.1. Geometrical model

Geometrical parameters are considered in this paper to investigate the flow characteristics and film distribution. Two horizontal tubes of a tube bundle used in a numerical model were built to simply study the falling effects on the first tube and its adjacent tube. The diameter of the circular tube is 19.05 mm. Because the geometrical model is axially symmetrical, to obtain effective results, the solution domain is chosen as simply half of an entire tube. In this paper, the tube walls are assumed to be completely wetted by liquid water. Fig. 1 shows an example schematic of a square-pitch tube bundle and corresponding grid model.

2.2. Assumptions and fluid properties

In this simulation, the Reynolds number varied from 600 to 1200, the flow regime was assumed to be laminar, and the flow pattern between adjacent horizontal tubes was a sheet flow. The critical Re number translated to the sheet flow from a column flow is about 550 [3,12]; however, the critical Re is 1600–1800 when the liquid film flow transits to a turbulent flow, which is typically $Re=4\Gamma/\mu$. The VOF model is applied to capture the interface of a multi-phase flow. The air is defined to be the primary phase, and liquid water is defined to be the secondary phase. This paper focuses on the falling film distribution covering the tubes, and thus, the heat transfer process and phase transition phenomenon are neglected. The properties of each phase are listed in Table 1.

2.3. Governing equations and VOF method

A continuity equation can be written in many ways for any material volume, for instance,

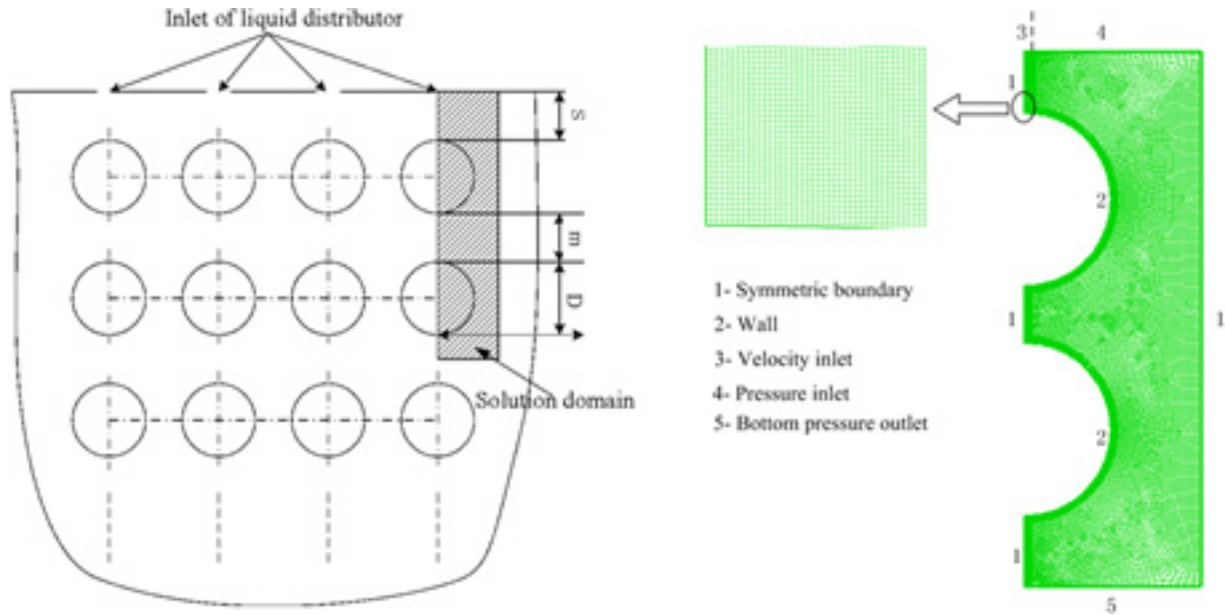


Fig. 1. Mesh used for two-dimensional model of square-pitch tube bundle.

Table 1
Summary of fluid properties used in computational analysis

	$\rho / \text{kg}\cdot\text{m}^{-3}$	$\mu / \text{kg}\cdot\text{m}^{-1}\cdot\text{s}^{-1}$	$\sigma / \text{N}\cdot\text{m}^{-1}$
Water-liquid	998.2	1×10^{-3}	0.073
Air	1.225	1.7894×10^{-5}	/

$$\nabla \cdot (\vec{v}) = 0 \tag{1}$$

where \vec{v} is the velocity vector.

$$\frac{\partial(\rho u)}{\partial t} + \frac{\partial(\rho u u)}{\partial x} + \frac{\partial(\rho u v)}{\partial y} = \frac{\partial}{\partial x} \left(\mu \frac{\partial u}{\partial x} \right) + \frac{\partial}{\partial y} \left(\mu \frac{\partial u}{\partial y} \right) - \frac{\partial p}{\partial x} + S_u \tag{2}$$

$$\frac{\partial(\rho v)}{\partial t} + \frac{\partial(\rho v u)}{\partial x} + \frac{\partial(\rho v v)}{\partial y} = \frac{\partial}{\partial x} \left(\mu \frac{\partial v}{\partial x} \right) + \frac{\partial}{\partial y} \left(\mu \frac{\partial v}{\partial y} \right) - \frac{\partial p}{\partial y} + S_v \tag{3}$$

where p is the pressure (Pa), μ is dynamic viscosity ($\text{kg}/\text{m}\cdot\text{s}$), S_u and S_v are the internal sources. The fluid is assumed to be of an incompressible viscous flow, and the viscosity is constant, $S_u = S_v = 0$.

The finite-volume method (FVM) is used to transfer these equations into algebraic expressions. The PISO method is chosen to relate the continuity equation to the pressure correction, and PRESTO discretization is adopted for the pressure. The mass and momentum equations are discretized using a second-order upwind scheme, and a Geo-Reconstruct scheme is adopted to solve the free-interface tracking.

In a VOF formulation, the continuity equation is modified to solve phase 2 (water).

$$\frac{\partial \alpha_2}{\partial t} + \vec{u} \cdot \nabla \alpha_2 = 0 \tag{4}$$

Then, the volume fraction equation for phase 1 (air) is

$$\alpha_1 = 1 - \alpha_2 \tag{5}$$

The density in the solution region can be expressed as

$$\rho = \alpha_2 \rho_L + (1 - \alpha_2) \rho_G \tag{6}$$

2.4. Sensitivity analysis

The sensitivities of the mesh number and time step were analyzed first to eliminate their effects on the simulation results. It was found that the average thickness of a liquid film tends to be constant when the mesh number increases and the time step decreases. When the mesh number is increased from 70147 to 111000, the calculated average film thickness only decreases by 0.2%. When the time step is decreased from 0.1 to 0.01 ms, the calculated average film thickness only decreases by 0.01%. This shows that the accuracy for the simulation applied in the present study can be ensured. Therefore, a grid number of 70,147 and time step of 0.1 ms were adopted to conduct the following calculations. Figs. 2 and 3 show verifications of the independence of the mesh and time-step, respectively. Here, D represents the outer diameter of a round tube, and s indicates the inter-tube spacing between the upper tube and its adjacent tube. In addition, the numerical results were also compared with the experiment results obtained by Gstoehl [20], and the theoretical results given by Nusselt [1]. The corresponding comparison results were presented in our previous work [13]. It was proved that a two-dimensional model using the VOF method is capable of capturing the thickness characteristics of the falling film of a sheet flow over a horizontal tube under adiabatic conditions. Therefore, this method is recommended in predicting the film thickness characteristics of a sheet flow

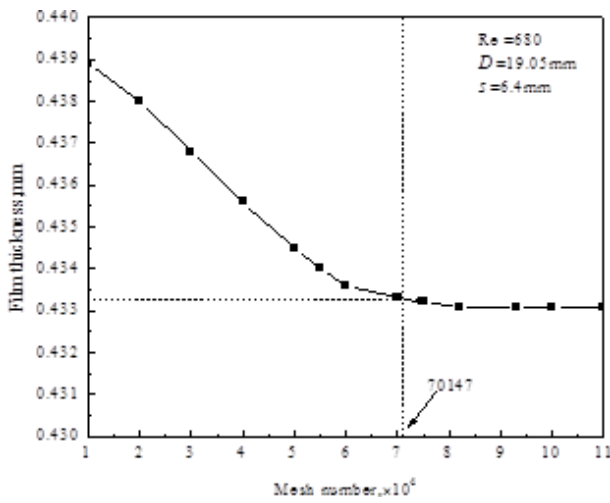


Fig. 2. Verification of mesh number independence.

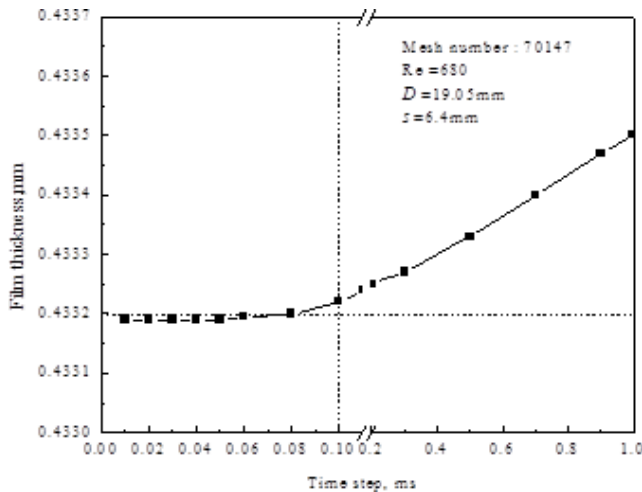


Fig. 3. Verification of time-step independence.

over a horizontal tube, and was adopted in the present study following previous researches on a falling film.

3. Results and discussion

The tube walls used in the simulation were defined to be completely wetted by liquid water in accordance with the practical multi-effect distillation process. The effects of the geometrical structure parameters on the flow characteristics and film distribution were studied, including the tube arrangement, inter-tube spacing, feeder height, and tube shape. The film thickness was measured exactly for a water volume fraction of 0.5. The model was solved using time steps of 0.1 ms, and the thickness calculated was the average value at a certain position at a particular instant.

3.1. Effects of tube arrangement on falling film distribution

The arrangement of a tube bundle will change the hydrodynamics of a falling film liquid, such as the shape

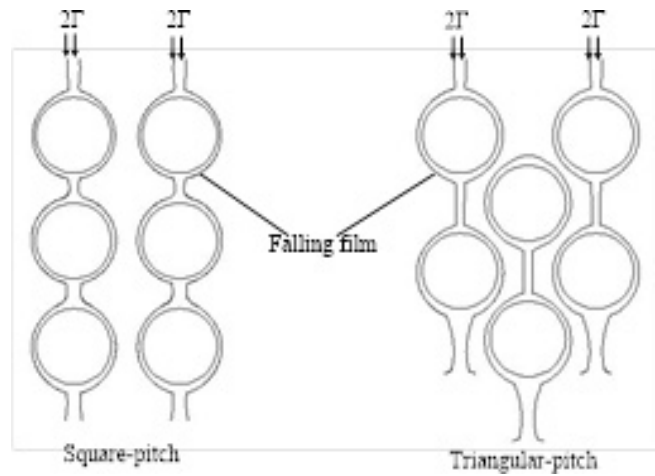


Fig. 4. Liquid film distributions in square-pitch and triangular-pitch tube bundle.

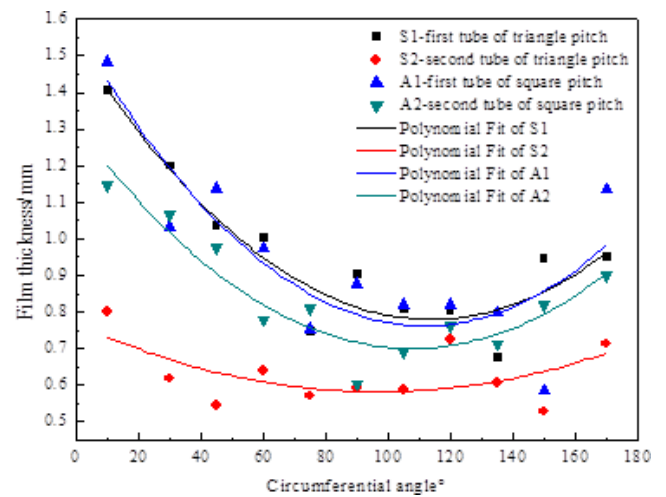


Fig. 5. Distribution curves of film thickness with different tube arrangements.

and velocity of the fluid. It also affects the exhaust of the vapor produced in the evaporator. The square-pitch and triangle-pitch arrangements of a tube bundle are widely used in practical equipment to obtain a uniform and stable falling liquid, as shown in Fig. 4.

The effects of the tube arrangement on the film distribution are presented in this paper. Fig. 5 illustrates the effects on the first and second tubes of a tube bundle. As shown in Fig. 5, the film distribution of the first tube is slightly different between the two types of arrangements. A distinct difference is shown between the two arrangements when the liquid falls over the second tube. It is clear that the second tube of a square-pitch arrangement has a thicker film than that of a triangle-pitch. The reasons for this might include the fact that the velocity of the fluid in a square-pitch arrangement is slower because the vertical distance between the tubes is shorter, which weakens the impact of a falling liquid and generates more liquid at equal times. On the contrary, when the inter-tube spacing is fixed, the ver-

tical distance of the triangle-pitch is larger. In addition, the impact of the liquid on the first tube is greater and the liquid film fluctuates more strongly and spreads more quickly. The film thickness covering the second tube will then be thinner when compared with a square-pitch arrangement.

3.2 Influence of inter-tube spacing on falling-film distribution

To investigate the influence of inter-tube spacing on the falling film distribution and film thickness covering a circular angle, four different cases of inter-tube spacing were chosen. Here, m indicates the ratio of inter-tube spacing to the tube diameter, the values of which are 1.1, 1.2, 1.4, and 1.6, respectively.

The film distribution of the first tube is shown in Fig. 6. The four curves of the film thickness are almost the same when m varies from 1.1 to 1.6. The liquid water sprays from the feeding system and falls over the first tube, and then continues falling owing to gravity and the surface tension. Normally, the distance between the sprayer and first tube is constant. Thus, the velocity of the falling liquid remains stable while the liquid adheres to the wall of the first tube, which is why the four curves nearly overlap in Fig. 6.

The ratio of inter-tube spacing to the tube diameter has a direct effect on the velocity of a falling liquid. With the increase in inter-tube spacing, the velocity of the liquid increases, and the impact action of liquid on the tube wall becomes stronger. Fig. 7 illustrates the distribution curves of the film thickness covering the second tube. In addition, the figure shows that the film thickness decreases with the increase in m . The film thickness is about 0.65 mm at a positional angle of 105° when m is 1.6, and becomes 0.93 mm at the same position when m is 1.1. This obvious difference indicates that the velocity changes rapidly for different spacing when the liquid falls to the second tube from the first. In addition, the impact of a falling liquid is much stronger with an increase in the inter-tube spacing. These hydrodynamic changes result in a noticeable trend regarding the thickness of the film on the second tube.

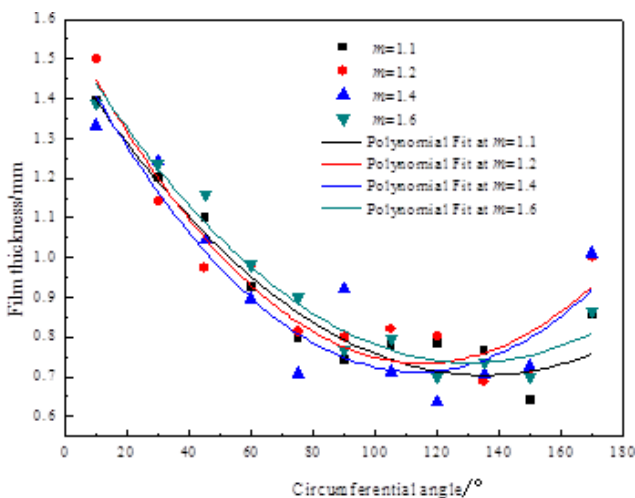


Fig. 6. Distribution curves of film thickness with different inter-tube spacing (first tube).

3.3. Effects of liquid feeder height on film distribution

To verify the role of hydrodynamics on velocity and impact, different cases of liquid feeder height were chosen to simulate the falling film distribution. The spray density was $0.3 \text{ kg/m}\cdot\text{s}$ and the liquid feeder heights (s) were 5, 8, 11, and 14 mm, respectively. Fig. 8 shows the changing trend for the different feeder height cases. With the increase in feeder height, the velocity and impact of the falling liquid increase in importance as the liquid adheres to the tube. Thus, the film thickness also decreases with the increase in liquid feeder height.

3.4. Influence of tube shape on film distribution

Three differently shaped tube models were built for a further investigation into the flow characteristics and film distribution outside a horizontal tube. The heat transfer

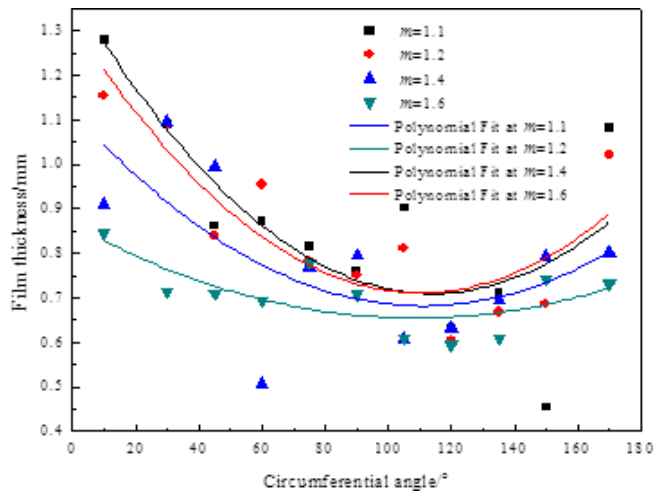


Fig. 7. Distribution curves of film thickness with different inter-tube spacing (second tube).

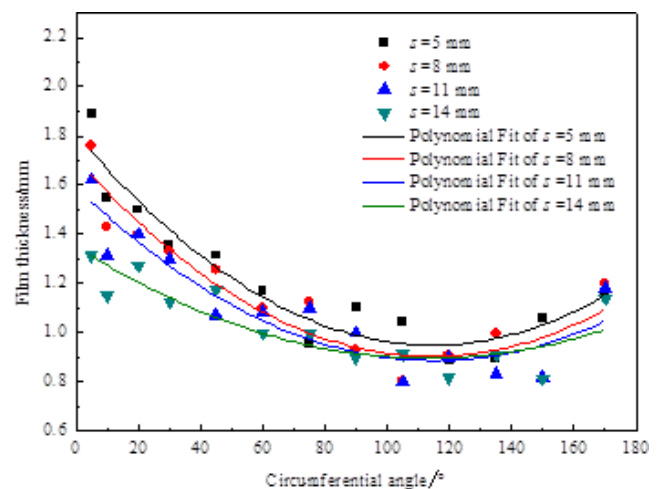


Fig. 8. Effect of liquid feeder height on the falling film distribution.

process takes place on the surface of the horizontal tubes in multi-effect desalination plants, and the magnitude of the horizontal tube surface area is the vital factor determining the heat exchange amount. Thus, the surface area of the elliptic tube selected as the model in this paper is a constant, and because this a simplified 2D model, the perimeter of the ellipse or circle should be constant, with the cross section of the horizontal tube also illustrated in the model.

Fig. 9 shows a physical model, where a represents the semi-major axis, and b indicates the semi-minor axis. The ratio of a to b is 1, 1.38, and 1.9 for the three different tube shapes, respectively, it should be noted that the tube is circular when a equals to b ($a/b = 1$). Table 2 lists the physical parameters of the three different tube shapes in the following simulations, where ϵ represents the ratio of the semi-major axis to the semi-minor axis.

Fig. 10 shows the falling film distribution and velocity distribution of a liquid film for the three different shapes tubes when the Reynolds number is 780. The left half of the figure is the gas-liquid phase distribution diagram, and the right half is the velocity contour diagram. The liquid film distribution was shown to be influenced by the gravity and viscosity forces in previous studies; in addition, the viscosity force obstructs the liquid film spread-

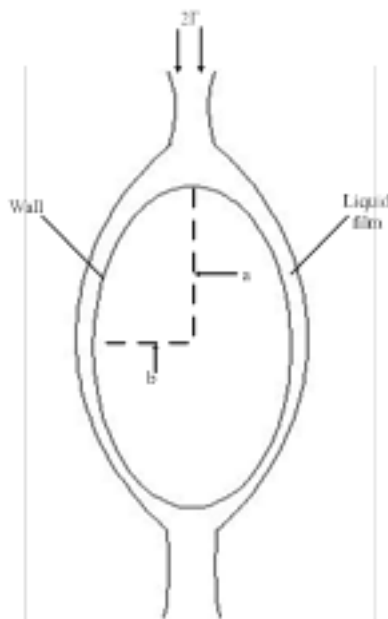
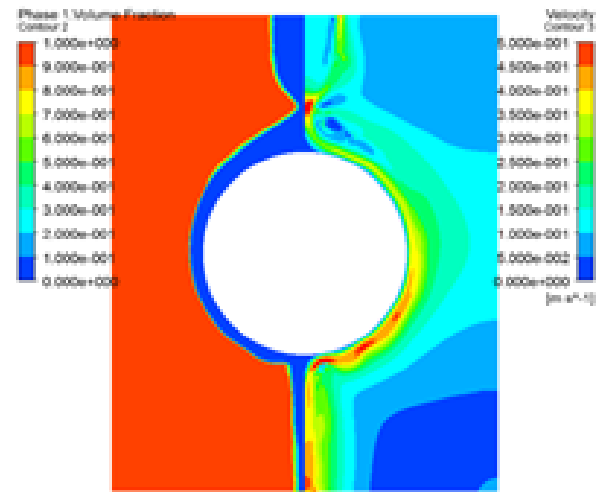


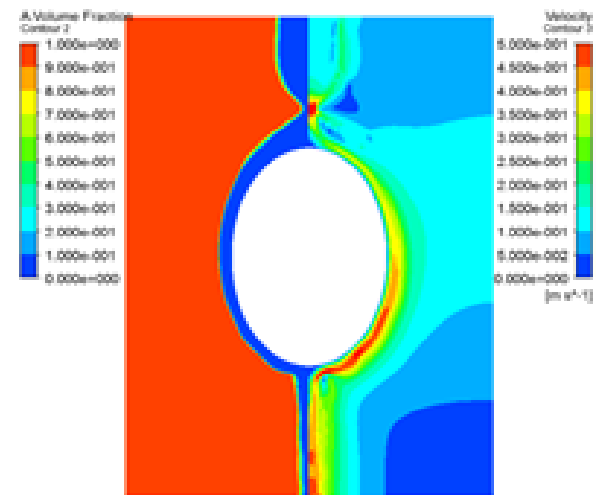
Fig. 9 Tube shape determined based on the parameters applied.

Table 2
Tube parameters of different shapes

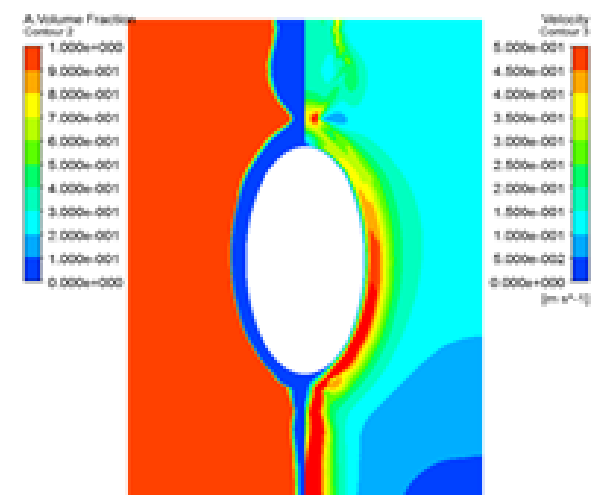
Parameters	Shape A	Shape B	Shape C
a/mm	9.5	10.6	11.5
b/mm	9.5	7.6	6
$\epsilon = a/b$	1	1.38	1.9



(a) shape A ($\epsilon = 1$)



(b) shape B ($\epsilon = 1.38$)



(c) shape C ($\epsilon = 1.9$)

Fig. 10. Comparison of film distribution outside different shaped tubes .

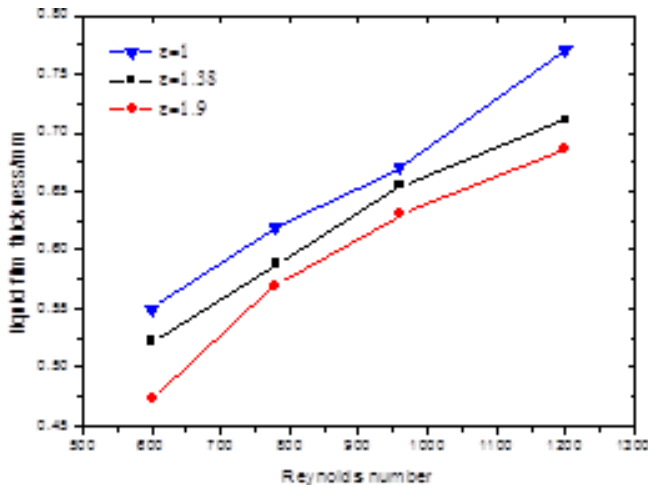


Fig. 11. Effects of Reynolds number on different tube shapes.

ing process along the revised direction, and the gravity force component of the flowing liquid in the tangential direction drives the liquid film spreading. For an elliptic tube shape, the greater the ratio of a to b is, the greater the gravity force component of the flowing liquid in the tangential direction, which results in a faster spread of the liquid film. The velocity contour is shown in Fig. 10, where the mass flow rate at the velocity inlet is constant, and the liquid film becomes thinner when the velocity of the liquid film increases. In other words, the tube shape influences the liquid film distribution, and the liquid film thickness decreases with an increase in the ellipticity.

To accurately present the differences in film thickness among the three types of tubes, four Reynolds numbers were simulated in this paper. Fig. 11 shows the film thickness distribution curves with the Re increasing at an angle of 90° when the process of the liquid film spread tends to be stable. It is clear that the film thickness increases with the increase in Reynolds number. Moreover, for the three different tubes, the film thickness of shape A ($\epsilon = 1$) is always the maximum, that of shape C ($\epsilon = 1.9$) is always the minimum, and that of shape B ($\epsilon = 1.38$) is the median. The results also illustrate that the tube shapes have a significant effect on the film distribution, and in the sheet flow, the liquid film thickness decreases as ϵ increases when the ellipse perimeter of the horizontal tube cross section is constant; in addition, a thinner liquid film can improve the heat exchange efficiency during the real heat transfer process for a laminar flow [21]. Thus, in the design of the tube shape of an HSFFE, it is worth considering that an elliptic tube is adaptable in replacing a standard circular tube.

4. Conclusions

The falling-film flow characteristics have crucial effects on the heat and mass transfer process in an evaporator. A 2D model was built to simulate the effects of the geometrical parameters, including the tube arrangement, inter-tube spacing, liquid feeder height, and tube shape on the flow characters. The film distribution along the first and second

rows of tubes was also analyzed in detail to illustrate the flow characteristics during the falling film process. The main conclusions are as follows:

- (1) The film distribution of the first row of tubes shows little difference between the two types of tube arrangements, but has a distinct difference when the liquid falls over the second row of tubes.
- (2) The inter-tube spacing directly determines the velocity of the falling liquid. The changes in hydrodynamics changes causes a noticeable trend of in terms of film thickness on the second row of tubes. The film thickness decreases with the increase of in inter-tube spacing.
- (3) The film thickness decreases with the increase in liquid feeder height when the flow density is constant.
- (4) The tube shape has a significant effect on the force condition and flow characteristics of a falling liquid. In the four cases of Reynolds number applied, the film thickness of shape A ($\epsilon = 1$) was consistently the maximum, that of shape C ($\epsilon = 1.9$) was always the minimum, and that of shape B ($\epsilon = 1.38$) was the median.

Symbols

a	—	Ellipse semi major axis, mm
b	—	Ellipse semi minor axis, mm
D	—	Outer diameter of round tube, mm
g	—	Acceleration of gravity, m/s^2
m	—	Ratio of inter-tube spacing to tube diameter
p	—	Pressure, Pa
Re	—	Reynolds number
s	—	Liquid feeder height, mm
S	—	Source item
t	—	Time, s
u	—	Velocity scale in x-direction
U	—	Velocity vector
v	—	Velocity scale in y-direction
x	—	Length scale
y	—	Length scale
α	—	Volume fraction
β	—	Circumferential angle, o
δ	—	Liquid film thickness, m
σ	—	Surface tension, N/m
μ	—	Dynamic viscosity, $kg/m \cdot s$
ν	—	Kinematic viscosity, m^2/s
Γ	—	Liquid film flow rate on one side per unit length of round tube, $kg/m \cdot s$
ρ	—	Density, kg/m^3

Subscript

1	—	Primary phase
2	—	Secondary phase
L	—	Liquid
G	—	Gas

Acknowledgments

The authors acknowledge the financial support of the National Natural Science Foundation of China (No. 51376035 and No. 51336001) and the Seawater Desalinated Key Laboratory in Liaoning province. The authors also thank the anonymous reviewers for their helpful comments and suggestions related to this paper.

References

- [1] W. Nusselt, Die Oberflächenkondensation des Wasserdampfes, *Zeitschr. Ver. Deut. Ing.*, 60 (1916) 541–546.
- [2] J.T. Rogers, S.S. Goindi, Experimental laminar falling film heat transfer coefficient on a large diameter horizontal tube, *Can. J. Chem. Eng.*, 67 (1989) 560–568.
- [3] X. Hu, A.M. Jacobi, The inter tube falling film: Part 1—flow characteristics, mode transitions, and hysteresis, *T. ASME*, 118 (1996) 616–625.
- [4] V. Slesarenko, Hydrodynamics and heat exchange during film evaporation of sea water in a vapor water up flow, *Desalination*, 33 (1980) 251–257.
- [5] G. Ribatski, A.M. Jacobi, Falling-film evaporation on horizontal tubes—a critical review, *Int. J. Refrig.*, 28 (2005) 635–653.
- [6] L. Xu, W. Shichang, Flowing state of liquid films over horizontal tubes and its influences on heat-transfer characteristics, *J. Chem. Ind. Eng.*, 53 (2002) 555–559.
- [7] L. Xu, Heat-transfer film coefficients of falling film horizontal tube evaporators, *Desalination*, 166 (2004) 223–230.
- [8] L. Harikrishnan, M.P. Maiya, Investigations on heat and mass transfer characteristics of falling film horizontal tubular absorber, *Int. J. Heat Mass Tran.*, 54 (2011) 2609–2617.
- [9] L. Harikrishnan, S. Tiwari, Numerical study of heat and mass transfer characteristics on a falling film horizontal tubular absorber for R-134a-DMAC, *Int. J. Therm. Sci.*, 50 (2011) 149–159.
- [10] H. Hou, Q.C. Bi, Distribution characteristics of falling film thickness around a horizontal tube, *Desalination*, 285 (2012) 393–398.
- [11] X.S. Mu, S.S. Shen, Experimental study of falling film evaporation heat transfer coefficient on horizontal tube, *Desal. Water Treat.*, 50 (2012) 310–316.
- [12] X. Chen, S.Q. Shen, Measurement on falling film thickness distribution around horizontal tube with laser-induced fluorescence technology, *Int. J. Heat Mass Tran.*, 89 (2015) 707–713.
- [13] Q.G. Qiu, X.J. Zhu, L. Mu, S.S. Shen, Numerical study of falling film thickness over fully wetted horizontal round tube, *Int. J. Heat Mass Tran.*, 84 (2015) 893–897.
- [14] V. Subramaniam, Numerical study of heat and mass transfer in lithium bromide-water falling films and droplets, *Int. J. Refrig.*, 40 (2014) 211–226.
- [15] E.W. Zavaleta-Aguilar, Horizontal tube bundle falling film distiller for ammonia–water mixtures, *Int. J. Refrig.*, 59 (2015) 304–316.
- [16] J.G. Bustamante, S. Garimella, Dominant flow mechanisms in falling-film and droplet-mode evaporation over horizontal rectangular tube banks, *Int. J. Refrig.*, 43 (2014) 80–89.
- [17] C.H. Qi, H.J. Feng, H.Q. Lv, C. Miao, Numerical and experimental research on the heat transfer of seawater desalination with liquid film outside elliptical tube, *Int. J. Heat Mass Tran.*, 93 (2016) 207–216.
- [18] E.A. Saleh, S.J. Ormiston, An elliptic two-phase numerical model of laminar film condensation from a steam-air mixture flowing over a horizontal tube, *Int. J. Heat Mass Tran.*, 112 (2017) 676–688.
- [19] C.Y. Zhao, W.T. Ji, Y.L. He, Y.J. Zhong, W.Q. Tao, A comprehensive numerical study on the sub-cooled falling film heat transfer on a horizontal smooth tube, *Int. J. Heat Mass Tran.*, 119 (2018) 259–270.
- [20] D. Gstoehl, J.F. Roques, P. Crisinel, J.R. Thome, Measurement of falling film thickness around a horizontal tube using a laser measurement technique, *Heat Transfer. Eng.*, 25 (2004) 28–34.
- [21] M. Xuehu, G. Dazhi, A. Jiaming, Experimental study on the heat transfer characteristics of the surface of the functional surface, *J. Therm. Sci. Tech-Jpn.*, 2 (2003) 119–123.